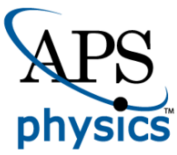

Topological Invariants for Quantum Quench Dynamics from Unitary Evolution

Haiping Hu and Erhai Zhao

Phys. Rev. Lett. **124**, 160402 — Published 21 April 2020

DOI: 10.1103/PhysRevLett.124.160402

Topological invariants for quantum quench dynamics from unitary evolution

Haiping Hu[1,2] and Erhai Zhao[1,*]

[1] *Department of Physics and Astronomy, George Mason University, Fairfax, Virginia 22030, USA*
[2] *Department of Physics and Astronomy, University of Pittsburgh, Pittsburgh, Pennsylvania 15260, USA*

(Dated: March 31, 2020)

Recent experiments began to explore the topological properties of quench dynamics, i.e. the time evolution following a sudden change in the Hamiltonian, via tomography of quantum gases in optical lattices. In contrast to the well established theory for static band insulators or periodically driven systems, at present it is not clear whether, and how, topological invariants can be defined for a general quench of band insulators. Previous work solved a special case of this problem beautifully using Hopf mapping of two-band Hamiltonians in two dimensions. But it only works for topologically trivial initial state and is hard to generalize to multiband systems or other dimensions. Here we introduce the concept of loop unitary constructed from the unitary time-evolution operator, and show its homotopy invariant fully characterizes the dynamical topology. For two-band systems in two dimensions, we prove that the invariant is precisely equal to the change in the Chern number across the quench regardless of the initial state. We further show that the nontrivial dynamical topology manifests as hedgehog defects in the loop unitary, and also as winding and linking of its eigenvectors along a curve where dynamical quantum phase transition occurs. This opens up a systematic route to classify and characterize quantum quench dynamics.

Introduction. Topological structures are ubiquitous in nature. They appear either in real space, e.g. a smoke ring or linked coronal loops near the Sun, or in momentum space, e.g. skymions in a Chern insulator or hedgehogs in a Weyl semimetal. Recently, the investigation of topological phenomena [1, 2] extended to time-dependent quantum systems, e.g. Floquet systems under periodic driving [3–13] or quench dynamics following a sudden change in the Hamiltonian, $H_0 \to H$ [14–30]. For these dynamical systems, the topological structures are hidden in the momentum-time continuum. Intriguingly, there seems a deep connection between the static band topology and quench dynamics. For example, topological insulators in integer classes can be systematically classified by quantum quenches starting from a trivial state based on the dynamical bulk-surface correspondence [21, 26]. Quench dynamics has been measured in details for example in experiments on ultracold atoms [31–33] and photonic quantum walks [34, 35]. This raises the question, how to systematically construct the topological invariants for the quench dynamics of band insulators?

The answer to this question remains open. Previous work on the quench dynamics of two-band Bloch Hamiltonians cast the problem mathematically as a Hopf map to arrive at a powerful result: the time evolution is characterized by the so-called Hopf invariant, which counts the linking number of the preimages of two time-evolved states, and equals to the Chern number of the post-quench Hamiltonian H [18]. Experimentally, such Hopf links in the momentum-time space have been observed using Bloch-state tomography for ultracold ^{40}K and ^{87}Rb atoms in optical lattices [31–33]. This framework based on Hopf mapping however works only for two-band Hamiltonians in two dimensions (2D). Moreover, it requires the pre-quench Hamiltonian H_0 to be topologically trivial. For quenches from a nontrivial state, the Hopf invariant is no longer well-defined [36–38]. Thus, a unified theory valid for general quench is still lacking. A proper topological invariant that remains well defined regardless of the triviality of the initial state is highly desired.

The quench dynamics of Chern insulators has also been studied from the perspective of dynamical quantum phase transition (DQPT) [39–50]. A DQPT is identified when physical observables show nonanalytic behavior at some time instant, e.g. when the post-quench state becomes orthogonal to the initial state [41]. It remains unclear how DQPT is related to the topological invariants for quench dynamics. Relatedly, periodically driven systems have been systematically classified into the periodic table of Floquet topological insulators [11, 12]. Possible connection between Floquet dynamics and quench dynamics, however, has not been noticed or emphasized.

To address these questions, we propose a new framework to characterize the topological properties of quench dynamics. We introduce the loop unitary U_l and show its homotopy invariant W_3 relates the pre- and post-quench Chern numbers by $W_3 = \mathcal{C}_f - \mathcal{C}_i$, which works for any H_0 and H. For trivial initial state, W_3 reduces to the Hopf invariant [18]. We reveal the origin of dynamical topology in the hedgehogs (π-defects) of the phase band of U_l. Moreover, we introduce the notion of DQPT curve to show the dynamical topology also manifests as the windings, links, or knots of the eigenvector of U_l along this curve. We illustrate our theory by applying it to a highly tunable model of two-band Hamiltonian in 2D. The framework paves the way to study the topological properties of more general quantum quenches.

Loop unitary for quantum quench. We will focus on the quantum quench dynamics of a generic two-band system

in 2D. The system starts from an arbitrary initial state $|\xi_0\rangle$ at time zero, then evolves according to a post-quench Hamiltonian $H = \boldsymbol{H}(\boldsymbol{k})\cdot\boldsymbol{\sigma}$, where the quasimomentum $\boldsymbol{k} = (k_x, k_y)$ and $\boldsymbol{\sigma} = (\sigma_x, \sigma_y, \sigma_z)$ is the Pauli matrix. At a later time τ, the state evolves into $|\xi(\tau)\rangle = e^{-iH\tau}|\xi_0\rangle$ with $\hbar = 1$. Let $\pm E_{\boldsymbol{k}}$ be the spectrum of H, and assume H is gapped, $E_{\boldsymbol{k}} > 0$. As far as the topological properties are concerned, we can rescale H and replace it with $h = H/E_{\boldsymbol{k}} = \hat{\boldsymbol{h}}(\boldsymbol{k})\cdot\boldsymbol{\sigma}$ where $\hat{\boldsymbol{h}}$ is a unit vector. This amounts to the standard band flattening. Equivalently, we can view $\boldsymbol{H} \to \hat{\boldsymbol{h}}$ as a rescaling of time $\tau \to t = E_{\boldsymbol{k}}\tau$. The rescaling yields a key observation: at $t = \pi$, the state returns to the initial state up to a minus sign, $|\xi(\pi)\rangle = -|\xi_0\rangle$. Thus, the quench dynamics has period π.

Previous works represent the two-component spinor $|\xi(t)\rangle$ with a point $\boldsymbol{\xi} = \langle\xi|\boldsymbol{\sigma}|\xi\rangle$ on the Bloch sphere S^2. This defines a mapping from the $(\boldsymbol{k}, t)$-space, a three-torus T^3, to S^2 with homotopy group $\pi_3(S^2) = \mathbb{Z}$ [51–53]. If the initial state $|\xi_0\rangle$ is topologically trivial with Chern number $\mathcal{C}_i = 0$, the quench dynamics can be characterized by the Hopf invariant as a Chern-Simons integral [18]

$$\mathcal{L} = \frac{1}{4\pi^2}\int_{\mathrm{T}^3} d^2\boldsymbol{k}dt\ \epsilon^{\mu\nu\rho}\mathcal{A}_\mu\partial_\nu\mathcal{A}_\rho. \tag{1}$$

Here $\mathcal{A}_\mu = i\langle\xi|\partial_\mu|\xi\rangle$ is the Berry connection, the indices $(\mu\nu\rho)$ take values in (k_x, k_y, t), and Einstein's summation convention is used. It is proved in Ref. [18] that $\mathcal{L} = \mathcal{C}_f$, where $\mathcal{C}_f$ is the post-quench Chern number. However, in general $\mathcal{C}_i \neq 0$, $\mathcal{L}$ is not well-defined [36–38]. Modified Chern-Simons integral can only give $(\mathcal{C}_f - \mathcal{C}_i)$ mod $2\mathcal{C}_i$ [37]. So new ideas are required to construct the invariant for generic quantum quenches.

We solve this problem by introducing the concept of loop unitary for quench dynamics. The unitary evolution does not have period π, $U(t = \pi) \neq \mathrm{I}$. However, it can be decomposed as the product of a loop unitary U_l that has time period π and the evolution of some constant Hamiltonian [11] where we must include information about the initial state or pre-quench Hamiltonian. This motivates us to define the following loop unitary operator

$$U_l(t) = e^{-iht}e^{ih_0t}, \tag{2}$$

where the first term on right is the time-evolution U, and h_0 is the pre-quench Hamiltonian with $|\xi_0\rangle$ as ground state: $h_0|\xi_0\rangle = -|\xi_0\rangle$. One can check that U_l indeed has period π, $U_l(0) = U_l(\pi) = \mathrm{I}$. In contrast to the $\mathrm{T}^3 \to S^2$ mapping above, U_l defines a mapping $\mathrm{T}^3 \to \mathrm{SU}(2)$ valid for arbitrary $|\xi_0\rangle$, h_0 and h. Then, the topological invariant for quench dynamics is the 3-winding number

$$W_3 = \frac{1}{24\pi^2}\int_{\mathrm{T}^3} d^2\boldsymbol{k}dt\ \epsilon^{\mu\nu\rho}\times \mathrm{Tr}[(U_l^{-1}\partial_\mu U_l)(U_l^{-1}\partial_\nu U_l)(U_l^{-1}\partial_\rho U_l)], \tag{3}$$

with $t \in [0, \pi]$. It is an integer following from homotopy group $\pi_3(\mathrm{SU}(2)) = \mathbb{Z}$. Note that $U_l(t)|\xi_0\rangle = e^{-it}|\xi(t)\rangle$ and $|\xi(t)\rangle$ represent the same state with different phase factors. It is easy to check W_3 reduces to Hopf invariant $\mathcal{L}$ when $|\xi_0\rangle$ is trivial, see [54, 59] for details.

π-defect in phase band. Now we are ready to relate W_3 to the Chern numbers $\mathcal{C}_{f,i}$. To this end, it is convenient to diagonalize U_l in its eigenbasis,

$$U_l(t) = e^{i\phi(\boldsymbol{k},t)}|\phi_+\rangle\langle\phi_+| + e^{-i\phi(\boldsymbol{k},t)}|\phi_-\rangle\langle\phi_-|. \tag{4}$$

Here $\pm\phi(\boldsymbol{k}, t)$ (with $0 \le \phi \le \pi$) are called phase bands, with $|\phi_\pm\rangle$ the corresponding eigenstates [11, 60]. We define spin vector $\pm\hat{\boldsymbol{m}} = \langle\phi_\mp|\boldsymbol{\sigma}|\phi_\mp\rangle$ from the phase bands, and note that U_l is homotopic [54] to a two-step evolution U_g given by $U_g = e^{-i2ht}$ for $0 < t < \frac{\pi}{2}$; $U_g = -e^{i2h_0(t-\frac{\pi}{2})}$ for $\frac{\pi}{2} < t < \pi$. Consequently U_l and U_g have the same topological properties and $W_3 = W_3[U_g]$. This relation reveals a deep connection between quantum quench and Floquet driving described by U_g. Via the phase bands of U_g, which are easier to work with, we can prove [54]

$$W_3 = \mathcal{C}_f - \mathcal{C}_i. \tag{5}$$

Hence W_3 gives the Chern number change and fully characterizes the quench. Compared to the Hopf invariant $\mathcal{L}$, W_3 is gauge-independent and valid for any initial state. Eqs. (3) and (5) are two key results of our paper.

The phase band analysis also provides an intuitive picture for the dynamical topology: W_3 counts the topological charge associated with the point degeneracies in the phase band [11, 60] at $\phi = \pi$, which we refer to as π-defects. These π-defects are located at special points in the $(\boldsymbol{k},t)$-space with $t = \frac{\pi}{2}$ and $\boldsymbol{k}$ determined by $\hat{\boldsymbol{h}} = \hat{\boldsymbol{n}}_0 = \langle\xi_0|\boldsymbol{\sigma}|\xi_0\rangle$, i.e., when the post-quench Hamiltonian vector $\hat{\boldsymbol{h}}$ is parallel to the initial spin vector $\hat{\boldsymbol{n}}_0$. Expanding U_l near a π-defect, we find it takes the form of Weyl Hamiltonian, e.g. $U_l(\delta k_x, \delta k_y, \delta t) = -\mathrm{I} - i\delta k_i K_{ij}\sigma_j$, with $\delta k_i \in (\delta k_x, \delta k_y, \delta t)$ being deviations from the degeneracy point. Such a Weyl point carries topological charge $\mathrm{sgn}(\det(K))$ [60]. We can show that W_3 counts the total charges of these π-defects [54]

$$W_3 = \frac{1}{8\pi}\sum\nolimits_P\int_{\boldsymbol{S}_P} d\boldsymbol{S}_P\cdot\ \epsilon^{ijk}(m_i\boldsymbol{\nabla}m_j\times\boldsymbol{\nabla}m_k). \tag{6}$$

Here $\boldsymbol{S}_P$ is a surface enclosing the π-defect, and the summation is over all π-defects. The phase-band spin vector $\hat{\boldsymbol{m}}$ forms a hedgehog [Fig. 1] around the π-defect.

Examples. To illustrate our theory, we apply it to a simple model with Hamiltonian $H_q = \boldsymbol{H}\cdot\boldsymbol{\sigma}$ given by

$$\begin{aligned} H_x + iH_y &= (\sin k_x + i\sin k_y)^q - R; \\ H_z &= M - \cos k_x - \cos k_y. \end{aligned} \tag{7}$$

At $R = 0$, the Chern number of the lower band $\mathcal{C} = q$ when $0 < M < 2$; $\mathcal{C} = -q$ when $-2 < M < 0$; and $\mathcal{C} = 0$ otherwise. When $q = 1$, the model reduces to the Qi-Wu-Zhang model [61] of 2D Chern insulators recently realized using ultracold atoms in optical Raman lattices

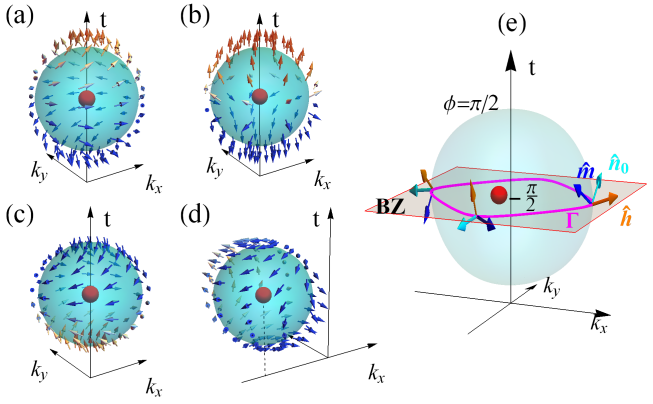

FIG. 1. Topological π-defects (solid red dots) as hedgehogs in the momentum-time space for quantum quenches. They are Weyl-like degeneracy points in the phase band of loop unitary U_l at $\phi = \pi$. The arrow denotes the phase-band spin vector $\hat{\boldsymbol{m}}$ near the defect. (a)-(b): quench from a trivial initial state $|\xi_0\rangle = (0,1)^T$ to $H_{q=1}$ and $H_{q=2}$ defined in model (7). (c)-(d): quench from the ground state of $H_{q=1}$ to $h = \sigma_z$ and $H_{q=2}$ respectively. The topological charge of the hedgehog is $+1, +2, -1, +1$ from (a) to (d), and equal to the Chern number change $\mathcal{C}_f - \mathcal{C}_i$ in each case. $R = 0$, $M = 1.6$. (e) Schematics of the DQPT curve Γ (magenta line). It is the intersection of the $t = \frac{\pi}{2}$ plane and the equal-ϕ surface of $\phi = \frac{\pi}{2}$ (green) which encloses the π-defect. Along Γ, vectors $\hat{\boldsymbol{n}}_0$, $\hat{\boldsymbol{h}}$ and $\hat{\boldsymbol{m}}$ are perpendicular to each other.

[62, 63]. We keep R, M as tuning parameters and assume $0 < M < 2$ below.

Let us consider four distinct quench pathways. The first two examples start from a trivial initial state $|\xi_0\rangle = (0,1)^T$ and quench to H_q above with $q = 1$ and $q = 2$ respectively. The π-defect for these cases is at $(k_x, k_y, t) = (0, 0, \frac{\pi}{2})$, and the hedgehog patterns of the $\boldsymbol{m}$-vector around the defect are depicted in Figs. 1(a)(b). For $q = 1$, expanding the loop unitary near the defect yields $U_l = -\mathrm{I} + i(d\delta k_y \sigma_x - d\delta k_x \sigma_y - 2\delta t \sigma_z)$ with $d = 1/(2 - M)$. The charge therefore is $+1$. For $q = 2$, the expansion yields a quadratic Weyl point [54] carrying charge $+2$. Next we consider quenches from the ground state of H_q with $q = 1$, i.e. from a topologically nontrivial initial state with $\mathcal{C}_i = 1$. In the third example, the post-quench Hamiltonian is trivial $h = \sigma_z$, $\mathcal{C}_f = 0$. We find a π-defect at $(0, 0, \frac{\pi}{2})$ with charge -1, see Fig. 1(c). In the fourth example, the post-quench Hamiltonian is H_q with $q = 2$, $\mathcal{C}_f = 2$. The π-defect is at $(-\arccos(M-1), 0, \frac{\pi}{2})$ with charge $+1$ as depicted in Fig. 1(d). One can check Eq. (5) indeed holds in all these four cases.

DQPT curve and winding number. The π-defects dictating the topology of quench dynamics reside in the 3D $(\boldsymbol{k},t)$-space. Next we show that the dynamical singularity also manifests along a lower dimensional curve, if the pre-quench (or post-quench) Hamiltonian is trivial. This provides another intuitive picture for the dynamical topology to reveal a deep connection to DQPT. A central concept in DQPT is Loschmidt echo (LE), which measures the overlap between the initial state and time-evolved state: $\mathcal{S}(t) = |\langle\xi_0|\xi(t)\rangle|^2$ [64]. The LE is equal to the squared average of the loop unitary operator over the initial state, $\mathcal{S}(t) = |\langle\xi_0|U_l(t)|\xi_0\rangle|^2$. Geometrically, after the quench, the spin vector $\boldsymbol{\xi}$ of the time-evolved state precesses around $\hat{\boldsymbol{h}}$. By definition, DQPT occurs when LE is zero, i.e. when $\boldsymbol{\xi}$ becomes anti-parallel to $\hat{\boldsymbol{n}}_0$. This requires $t = \frac{\pi}{2}$ and $\hat{\boldsymbol{h}} \perp \hat{\boldsymbol{n}}_0$, as depicted in Fig. 1(e). All the points satisfying these two conditions constitute a closed curve Γ on the $t = \frac{\pi}{2}$ plane, dubbed the DQPT curve. One can check that for points along Γ, the eigenphase of U_l takes $\phi = \frac{\pi}{2}$. Hence Γ is also the intersection of the equal-ϕ surface with $\phi = \frac{\pi}{2}$ and the $t = \frac{\pi}{2}$ plane, as illustrated in Fig. 1(e).

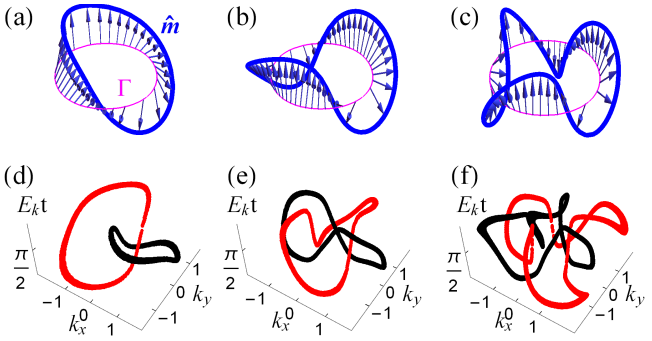

FIG. 2. (a)-(c): Winding of the phase-band spin vector $\hat{\boldsymbol{m}}$ (arrows) along the DQPT curve Γ for quench from initial state $|\xi_0\rangle = (0,1)^T$ to H_q with $q = 1, 2, 3$ (left to right). The corresponding winding number as defined in Eq. (8) is $\nu = 1, 2, 3$. (d)-(f): Hopf links in momentum-time space for the same quench to H_q with $q = 1, 2, 3$ (left to right). Shown are preimages of two time-evolved states $\pm\boldsymbol{\xi} = (1, 0, 0)$. $R = 0.2$, $M = 1.6$.

Suppose Γ is parameterized by some angle $\theta \in [0, 2\pi]$. Along Γ, the phase-band spin vector is given by $\hat{\boldsymbol{m}} = \hat{\boldsymbol{h}} \times \hat{\boldsymbol{n}}_0$, which in general tilts as θ is varied. By a unitary transformation $V^\dagger h_0 V = \sigma_z$, U_l becomes $V^\dagger U_l V = i(\tilde{m}_x \sigma_x + \tilde{m}_y \sigma_y)$. Hence the vector $\hat{\boldsymbol{m}}$ is fully described by polar angle $\chi = \arctan(\tilde{m}_y/\tilde{m}_x)$, and its round trip along Γ is characterized by the winding number

$$\nu = \frac{1}{2\pi} \oint_\Gamma d\theta \; \partial_\theta \chi. \tag{8}$$

One can further prove [54] that ν coincides with $\mathcal{C}_f$, and by the chain of identities established above it is also equal to W_3 and $\mathcal{L}$, when the initial state is trivial.

The winding of $\hat{\boldsymbol{m}}$ is illustrated in Fig. 2 for our model (7) with initial state $|\xi_0\rangle = (0,1)^T$. The DQPT curve in this case is given by $M - \cos k_x - \cos k_y = 0$. We plot $(\tilde{m}_x, \tilde{m}_y)$ as a vector on the local x-y plane normal to Γ. Figs. 2(a)-(c) illustrate the winding of $\hat{\boldsymbol{m}}$ for $q = 1, 2, 3$, respectively. By traveling counterclockwise along Γ, one observes that $\hat{\boldsymbol{m}}$ winds $1, 2, 3$ times within the x-y plane, in agreement with the calculation $\nu = q$. For comparison,

we have chosen two arbitrary states and plotted their preimages in the $(\boldsymbol{k}, t)$-space in Figs. 2(d)-(f). The two preimages form a Hopf link with linking number $\mathcal{L} = 1, 2, 3$, respectively, consistent with ν above.

Torus links and knots. Next we discuss quench from a trivial state to a Hamiltonian H with Dirac points, i.e. band degeneracies at certain isolated $\boldsymbol{k}$ points. To this end, it is useful to imagine a torus (pipe) of unit cross-sectional radius extending along Γ. Then the end points of $\hat{\boldsymbol{m}}$ trace out a curve Γ_+ on the torus surface. Similarly $-\hat{\boldsymbol{m}}$ traces out another curve Γ_-. For fully gapped H, the Gauss linking number of these two closed curves, $\Gamma_\pm$, is nothing but ν. If band degeneracies exist, one can verify that all Dirac points lie on Γ projected onto the Brillouin zone. At each Dirac point, the two phase bands $|\phi_\pm\rangle$ become degenerate. The net effect of the band touching is the role switch $\hat{\boldsymbol{m}} \leftrightarrow -\hat{\boldsymbol{m}}$. At the Dirac points, the curves $\Gamma_\pm$ continue smoothly, only to switch their characters there, $\Gamma_+ \leftrightarrow \Gamma_-$. It follows that $\Gamma_\pm$ together form either torus links or torus knots [65].

This can be illustrated by using our model Eq. (7). When $R = [1-(M-1)^2]^{3/2}$ for $q = 3$, one of the Weyl charges touches Γ at the Dirac point, while the other two charges remain inside as depicted in Fig. 3(a). The corresponding $\Gamma_\pm$ curves are projected onto a 2D plane for clarity. In this case, the $\Gamma_+ \leftrightarrow \Gamma_-$ switch happens only once. Together they form a single closed curve, a torus knot with crossing number $c_K = 5$. A different scenario is shown in Fig. 3(b) for $q = 2$ where H has one pair of Dirac points. The switch occurs twice to give rise to two curves. They form a torus link with linking number $c_L = 1$.

The invariants for these links and knots can be obtained as follows. Without loss of generality, we can treat H with Dirac points as the critical boundary between two gapped Hamiltonians with Chern number $\mathcal{C}_<$ and $\mathcal{C}_>$ respectively as some tuning parameter (e.g. R) is varied. In the first scenario, $\mathcal{C}_> - \mathcal{C}_< = odd$, i.e., there are odd number of Dirac points on Γ, leading to odd times of $\pm\hat{\boldsymbol{m}}$ switch and the formation of a torus knot [Fig. 3(a)]. Its crossing number [65] is then $c_K = 2\mathcal{C}_< + \mathcal{C}_> - C_< = \mathcal{C}_< + \mathcal{C}_>$. In the second scenario, $\mathcal{C}_> - \mathcal{C}_< = even$ with even number of Dirac points on Γ. Accordingly, $\pm\hat{\boldsymbol{m}}$ form a torus link [Fig. 3(b)], and its linking number is half the crossing number [65], $c_L = (\mathcal{C}_< + \mathcal{C}_>)/2$. These general results agree with the examples above. For $q = 3$, $\mathcal{C}_< = 3$ and $\mathcal{C}_> = 2$ to give $c_K = 5$; while for $q = 2$, $\mathcal{C}_< = 2$ and $\mathcal{C}_> = 0$ so $c_L = 1$. Thus, the concepts of loop unitary and DQPT curve also provide insights for quench to Dirac semimetals.

Outlook. In summary, we establish a new framework to characterize the topological properties of quench dynamics by introducing loop unitary U_l and its homotopy invariant W_3, which goes beyond the Hopf mapping and is independent of initial state. The dynamical topology is revealed pictorially in two ways, the π-defects in the phase bands, and the winding of $\hat{\boldsymbol{m}}$ along the DQPT curve. The theory is generalized further to discuss the link and knot structures for quench into critical Dirac semimetal. A series of identities are proved to relate the Chern, crossing, linking, and winding number.

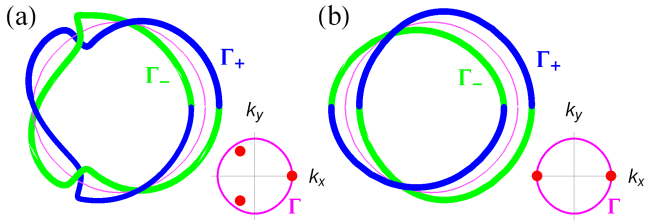

FIG. 3. Top view of a knot (a) and a link (b) formed by two curves $\Gamma_\pm$ traced by vector $\pm\hat{\boldsymbol{m}}$ along Γ for quenches to critical H_q with Dirac points. The insets show the topological charges on the $t = \pi/2$ plane. They cross Γ exactly at the Dirac points where the two curves switch, $\Gamma_+ \leftrightarrow \Gamma_-$. (a): A single curve ties into a knot with crossing number $c_K = 5$, $q = 3$, $R = 0.512$. (b): Two closed curves form a torus link with linking number $c_L = 1$, $q = 2$, $R = 0.64$. $M = 1.6$.

For concreteness, we have focused on the dynamics of two-band Hamiltonians in 2D. Our scheme based on the loop unitary however is general. For example, we have applied it to obtain the $\mathbb{Z}_2$ dynamical invariant for the quench dynamics of Hopf insulators [66] in 3D, and characterize the quench dynamics of the four-band Bernevig-Hughes-Zhang model [54]. For these more complicated cases, the loop unitary must be chosen to be time-periodic to ensure a closed base manifold, and the additional symmetry constraints must be properly taken into account [54] in constructing the desired dynamical topological invariants. Through the concept of loop unitary and homotopy relation $U_l \sim U_g$, our work also reveals an intrinsic connection between quench and Floquet dynamics [11, 12]. It suggests that a wealth of link and knot structures will also emerge in $(\boldsymbol{k}, t)$-space in Floquet systems. For example, Hopf link was recently shown to appear in periodically driven 2D systems [59].

Recent experiments have begun to quantitatively access quench dynamics via time- and momentum-resolved tomography [67–70]. In particular, spatiotemporal Hopf links [31–33] after quantum quench have been observed. The π-defect in the phase band can be observed via the same Bloch-state tomography technique. For example, its topological charge, which is quantized and protected against small perturbations, can be extracted locally from the nearby tomography points [71]. The location of the DQPT curve and the winding along it can be verified by tracing the emergent dynamical vortices in momentum space as done in Ref. [50]. For more details, see Supplementary Materials [54].

This work is supported by AFOSR Grant No. FA9550-16-1-0006 and NSF Grant No. PHY-1707484.

* ezhao2@gmu.edu

[1] M. Z. Hasan and C. L. Kane, *Colloquium*: Topological insulators, Rev. Mod. Phys. **82**, 3045 (2010).

[2] X.-L. Qi and S.-C. Zhang, Topological insulators and superconductors, Rev. Mod. Phys. **83**, 1057 (2011).

[3] T. Kitagawa, E. Berg, M. Rudner, and E. Demler, Topological characterization of periodically driven quantum systems, Phys. Rev. B **82**, 235114 (2010).

[4] N. H. Lindner, G. Rafael and V. Galitski, Floquet topological insulator in semiconductor quantum wells, Nat. Phys. **7**, 490495 (2011).

[5] L. Jiang, T. Kitagawa, J. Alicea, A. R. Akhmerov, D. Pekker, G. Refael, J. I. Cirac, E. Demler, M. D. Lukin, and P. Zoller, Majorana Fermions in Equilibrium and in Driven Cold-Atom Quantum Wires, Phys. Rev. Lett. **106**, 220402 (2011).

[6] M. S. Rudner, N. H. Lindner, E. Berg, and M. Levin, Anomalous Edge States and the Bulk-Edge Correspondence for Periodically Driven Two-Dimensional Systems, Phys. Rev. X **3**, 031005 (2013).

[7] A. Gómez-León and G. Platero, Floquet-Bloch Theory and Topology in Periodically Driven Lattices, Phys. Rev. Lett. **110**, 200403 (2013).

[8] L. DAlessio and M. Rigol, Dynamical preparation of Floquet Chern insulators, Nat. Commun. **6**, 8336 (2015).

[9] A. C. Potter, T. Morimoto, and A. Vishwanath, Classification of Interacting Topological Floquet Phases in One Dimension, Phys. Rev. X **6**, 041001 (2016).

[10] H. Hu, B. Huang, E. Zhao, and W. V. Liu, Dynamical Singularities of Floquet Higher-Order Topological Insulators, Phys. Rev. Lett. **124**, 057001 (2020).

[11] R. Roy and F. Harper, Periodic table for Floquet topological insulators, Phys. Rev. B **96**, 155118 (2017).

[12] S. Yao, Z. Yan, and Z. Wang, Topological invariants of Floquet systems: General formulation, special properties, and Floquet topological defects, Phys. Rev. B **96**, 195303 (2017).

[13] K. Yang et al., Floquet dynamical quantum phase transitions, Phys. Rev. B **100**, 085308 (2019).

[14] M. D. Caio, N. R. Cooper, and M. J. Bhaseen, Quantum Quenches in Chern Insulators, Phys. Rev. Lett. **115**, 236403 (2015).

[15] Y. Hu, P. Zoller, and J. C. Budich, Dynamical Buildup of a Quantized Hall Response from Nontopological States, Phys. Rev. Lett. **117**, 126803 (2016).

[16] J. H. Wilson, J. C. W. Song, and G. Rafael, Remnant Geometric Hall Response in a Quantum Quench, Phys. Rev. Lett. **117**, 235302 (2016).

[17] M. D. Caio, N. R. Cooper, and M. J. Bhaseen, Hall response and edge current dynamics in Chern insulators out of equilibrium, Phys. Rev. B **94**, 155104 (2016).

[18] C. Wang, P. Zhang, X. Chen, J. Yu, and H. Zhai, Scheme to Measure the Topological Number of a Chern Insulator from Quench Dynamics, Phys. Rev. Lett. **118**, 185701 (2017).

[19] C. Yang, L. Li, and S. Chen, Dynamical topological invariant after a quantum quench, Phys. Rev. B **97**, 060304(R) (2018).

[20] Z. Gong and M. Ueda, Topological Entanglement-Spectrum Crossing in Quench Dynamics, Phys. Rev. Lett. **121**, 250601 (2018).

[21] L. Zhang, L. Zhang, S. Niu, and X.-J. Liu, Dynamical classification of topological quantum phases, Science Bulletin **63** (21), 1385-1391 (2018).

[22] J. Yu, Phase vortices of the quenched Haldane model, Phys. Rev. A **96**, 023601 (2017).

[23] P.-Y. Chang, Topology and entanglement in quench dynamics, Phys. Rev. B **97**, 224304 (2018).

[24] M. Ezawa, Topological quantum quench dynamics carrying arbitrary Hopf and second Chern numbers, Phys. Rev. B **98**, 205406 (2018).

[25] J. Yu, Measuring Hopf links and Hopf invariants in a quenched topological Raman lattice, Phys. Rev. A **99**, 043619 (2019).

[26] L. Zhang, L. Zhang, X.-J. Liu, Characterizing topological phases by quantum quenches: A general theory, Phys. Rev. A **100**, 063624 (2019).

[27] L. Zhang, L. Zhang, and X.-J. Liu, Dynamical detection of topological charges, Phys. Rev. A **99**, 053606 (2019).

[28] T. Nag, V. Juričić, and B. Roy, Out of equilibrium higher-order topological insulator: Floquet engineering and quench dynamics, Phys. Rev. Research **1**, 032045(R) (2019).

[29] D. Toniolo, Time-dependent topological systems: A study of the Bott index, Phys. Rev. B **98**, 235425 (2018).

[30] R. Jafari, Henrik Johannesson, A. Langari, and M. A. Martin-Delgado, Quench dynamics and zero-energy modes: The case of the Creutz model, Phys. Rev. B **99**, 054302 (2019).

[31] M. Tarnowski, F. Nur Ünal, N. Fläschner, B. S. Rem, A. Eckardt, K. Sengstock, C. Weitenberg, Measuring topology by dynamics: Chern number from linking number, Nat. Commun. **10**, 1728 (2019).

[32] W. Sun, C.-R. Yi, B.-Z. Wang, W.-W. Zhang, B. C. Sanders, X.-T. Xu, Z.-Y. Wang, J. Schmiedmayer, Y. Deng, X.-J. Liu, S. Chen, and J.-W. Pan, Uncover Topology by Quantum Quench Dynamics, Phys. Rev. Lett. **121**, 250403 (2018).

[33] C.-R. Yi, J.-L. Yu, W. Sun, X.-T. Xu, S. Chen, J.-W. Pan, Observation of the Hopf Links and Hopf Fibration in a 2D topological Raman Lattice, arXiv:1904.11656.

[34] K. Wang, X. Qiu, L. Xiao, X. Zhan, Z. Bian, B. C. Sanders, W. Yi, and P. Xue, Observation of emergent momentum–time skyrmions in parity–time-symmetric non-unitary quench dynamics, Nat. Commun. **10**, 2293 (2019).

[35] K. Wang, X. Qiu, L. Xiao, X. Zhan, Z. Bian, W. Yi, and P. Xue, Simulating Dynamic Quantum Phase Transitions in Photonic Quantum Walks, Phys. Rev. Lett. **122**, 020501 (2019).

[36] F. Wilczek and A. Zee, Linking Numbers, Spin, and Statistics of Solitons, Phys. Rev. Lett. **51**, 2250 (1983).

[37] X. Chen, C. Wang, J. Yu, Linking invariant for the quench dynamics of a two-dimensional two-band Chern insulator, Phys. Rev. A **101**, 032104 (2020).

[38] J. C. Y. Teo and C. L. Kane, Topological defects and gapless modes in insulators and superconductors, Phys. Rev. B **82**, 115120 (2010).

[39] M. Heyl, A. Polkovnikov, and S. Kehrein, Dynamical Quantum Phase Transitions in the Transverse-Field Ising Model, Phys. Rev. Lett. **110**, 135704 (2013).

[40] M. Heyl, Scaling and Universality at Dynamical Quantum Phase Transitions, Phys. Rev. Lett. **115**, 140602 (2015).

[41] M. Heyl, Dynamical quantum phase transitions: a review, Rep. Prog. Phys. **81**, 054001 (2018).

[42] S. Vajna and B. Dóra, Topological classification of dynamical phase transitions, Phys. Rev. B **91**, 155127 (2015).

[43] J. C. Budich and M. Heyl, Dynamical topological order parameters far from equilibrium, Phys. Rev. B **93**, 085416 (2016).

[44] Z. Huang and A. V. Balatsky, Dynamical Quantum Phase Transitions: Role of Topological Nodes in Wave Function Overlaps, Phys. Rev. Lett. **117**, 086802 (2016).

[45] X. Qiu, T.-S. Deng, G.-C. Guo, and W. Yi, Dynamical topological invariants and reduced rate functions for dynamical quantum phase transitions in two dimensions, Phys. Rev. A **98**, 021601(R) (2018).

[46] J. Lang, B. Frank, and J. C. Halimeh, Dynamical Quantum Phase Transitions: A Geometric Picture, Phys. Rev. Lett. **121**, 130603 (2018).

[47] P. Uhrich, N. Defenu, R. Jafari, J. C. Halimeh, Out-of-equilibrium phase diagram of long-range superconductors, ArXiv:1910.10715.

[48] P. Jurcevic, H. Shen, P. Hauke, C.Maier, T. Brydges, C. Hempel, B. P. Lanyon, M. Heyl, R. Blatt, and C. F. Roos, Direct Observation of Dynamical Quantum Phase Transitions in an Interacting Many-Body System, Phys. Rev. Lett. **119**, 080501 (2017).

[49] J. Zhang, G. Pagano, P. W. Hess, A. Kyprianidis, P. Becker, H. Kaplan, A. V. Gorshkov, Z.-X. Gong, and C. Monroe, Observation of a many-body dynamical phase transition with a 53-qubit quantum simulator, Nature **551**, 601604 (2017).

[50] N. Fläschner, D. Vogel, M. Tarnowski, B. S. Rem, D.-S. Lühmann, M. Heyl, J. C. Budich, L. Mathey, K. Sengstock, and C. Weitenberg, Observation of dynamical vortices after quenches in a system with topology, Nat. Phys. **14**, 265 (2018).

[51] J. E. Moore, Y. Ran, and X.-G. Wen, Topological Surface States in Three-Dimensional Magnetic Insulators, Phys. Rev. Lett. **101**, 186805 (2008).

[52] D.-L. Deng, S.-T. Wang, C. Shen, and L.-M. Duan, *Hopf insulators and their topologically protected surface states*, Phys. Rev. B **88**, 201105(R) (2013).

[53] D.-L. Deng, *Topological Phases of Matter: Classification, Realization and Application,* PhD thesis, 2015.

[54] See Supplementary Material for more details on (I) the relation between W_3 and Hopf invariant $\mathcal{L}$; (II) homotopy relation of loop unitary; (III) phase-band representation; (IV) π-defect and Weyl charge; (V) winding topology of DQPT curve; (VI) dynamical topology of BHZ model; and (VII) experimental detection of DQPT curve and topological charge, which includes Refs. [55–58].

[55] M Nakahara, *Geometry, Topology and Physics* (Second Edition, Taylor and Francis, 2003).

[56] B. A. Bernevig, T. L. Hughes, and S.-C. Zhang, Quantum Spin Hall Effect and Topological Phase Transition in HgTe Quantum Wells, Science **314**, 1757 (2006).

[57] L. Fu and C. L. Kane, Topological insulators with inversion symmetry, Phys. Rev. B **76**, 045302 (2007).

[58] D. Carpentier, P. Delplace, M. Fruchart, and K. Gawedzki, Topological Index for Periodically Driven Time-Reversal Invariant 2D Systems, Phys. Rev. Lett. **114**, 106806 (2015).

[59] F. N. Ünal, A. Eckardt, R.-J. Slager, Hopf characterization of two-dimensional Floquet topological insulators, Phys. Rev. Research **1**, 022003(R) (2019).

[60] F. Nathan and M. S Rudner, Topological singularities and the general classification of FloquetBloch systems, New J. Phys. **17**, 125014 (2015).

[61] X.-L. Qi, Y.-S. Wu, and S.-C. Zhang, Topological quantization of the spin Hall effect in two-dimensional paramagnetic semiconductors, Phys. Rev. B **74**, 085308 (2006).

[62] Z. Wu, L. Zhang, W. Sun, X.-T. Xu, B.-Z. Wang, S.-C. Ji, Y. Deng, S. Chen, X.-J. Liu, and J.-W. Pan, Realization of two-dimensional spin-orbit coupling for Bose-Einstein condensates, Science **354**, 83 (2016).

[63] W. Sun, B.-Z. Wang, X.-T. Xu, C.-R. Yi, L. Zhang, Z. Wu, Y. Deng, X.-J. Liu, S. Chen, and J.-W. Pan, Highly Controllable and Robust 2D Spin-Orbit Coupling for Quantum Gases, Phys. Rev. Lett. **121**, 150401 (2018).

[64] A. Peres, Stability of quantum motion in chaotic and regular systems, Phys. Rev. A **30**, 1610 (1984).

[65] K. Murasugi, *Knot theory and its applications* (Springer Science and Business Media, 2007).

[66] H. Hu, C. Yang, and E. Zhao, Quench Dynamics of Hopf Insulators, arXiv:1912.03436.

[67] P. Hauke, M. Lewenstein, and A. Eckardt, Tomography of Band Insulators from Quench Dynamics, Phys. Rev. Lett. **113**, 045303 (2014).

[68] N. Fläschner, B. S. Rem, M. Tarnowski, D. Vogel, D.-S. Lühmann, K. Sengstock, and C. Weitenberg, Experimental reconstruction of the Berry curvature in a Floquet Bloch band, Science **352**, 1091-1094 (2016).

[69] T. Li, L. Duca, M. Reitter, F. Grusdt, E. Demler, M. Endres, M. Schleier-Smith, I. Bloch, U. Schneider, Bloch state tomography using Wilson lines, Science **352**, 1094 (2016).

[70] E. Alba, X. Fernandez-Gonzalvo, J. Mur-Petit, J. K. Pachos, and J. J. Garcia-Ripoll, Seeing Topological Order in Time-of-Flight Measurements, Phys. Rev. Lett. **107**, 235301 (2011).

[71] F. N. Ünal, B. Seradjeh, and A. Eckardt, How to Directly Measure Floquet Topological Invariants in Optical Lattices, Phys. Rev. Lett. **122**, 253601 (2019).